Chemical Functionalization of the Zinc Selenide Surface and Its Impact on Lactobacillus rhamnosus GG Biofilms

Elena Yunda, Halima Alem, Gregory Francius, Raúl Gago, Fabienne Quilès

ACS Applied Materials & Interfaces, 12(13), 14933-14945 (2020). DOI:10.1021/acsami.0c01335

Chemical functionalization of the zinc selenide surface and its impact on *Lactobacillus rhamnosus* GG biofilms

Elena Yunda[a,b], Halima Alem[b,c], Grégory Francius[a], Raúl Gago[d], Fabienne Quilès[a]*

[a] Laboratoire de Chimie Physique et Microbiologie pour les Matériaux et l'Environnement, LCPME, UMR 7564 Université de Lorraine-CNRS, 405, rue de Vandoeuvre, 54600 Villers-lès-Nancy, France

[b] Institut Jean Lamour, IJL, UMR 7198 Université de Lorraine-CNRS, Campus Artem, 2 allée André Guinier, 54000 Nancy, France

[c] Institut Universitaire de France, 1, rue Descartes, 75231 Paris, France

[d] Instituto de Ciencia de Materiales de Madrid, Consejo Superior de Investigaciones Científicas, Campus de Cantoblanco, Calle Sor Juana Inés de la Cruz, 3, 28049 Madrid, Spain

KEYWORDS

Surface functionalization, bacteria, *Lactobacillus rhamnosus* GG, ATR-FTIR, self-assembled monolayers, zinc selenide.

ABSTRACT

Bacteria grow on surfaces and form communities called biofilms. Bacterial adhesion and properties of the derived biofilms depend on, among others, the nature of the supporting substrate. Here, we report how the surface properties of the substrate affect the biofilm growth of probiotic *Lactobacillus rhamnosus* GG (LGG). Hydrophilic (OH), hydrophobic (CH_3) and positively charged (NH_3^+) surfaces were obtained by the functionalization of a ZnSe crystal with alkanethiol self-assembled monolayers (SAM). The self-assembly of alkanethiols onto ZnSe was studied *in situ* using infrared spectroscopy in Attenuated Total Reflection mode (ATR-FTIR). The organization of grafted SAMs was analyzed based on the results of ATR-FTIR, high-energy elastic backscattering spectrometry, and contact angle measurements. The kinetics and adhesion strength of LGG initial attachment as well as its physiological state on surfaces terminated by the different functional groups were assessed by the combination of ATR-FTIR, force measurements based on atomic force microscopy, and fluorescent staining of bacteria. The strength of interactions between LGG and the surface was strongly affected by the terminal group of the alkanethiol chain. The -NH_3^+ groups displayed the highest affinity with LGG at the first stage of interaction. The surface properties also played an important role when LGG biofilms were further grown in a nutritive medium for 24 hours under flow conditions. Notably, the analysis of the infrared spectra recorded during the biofilm cultivation revealed differences in the kinetics of growth and in the polysaccharide features of the biofilm depending on the substrate functionality. LGG biofilm was stable only on the positively charged surface upon rinsing. Findings of this work clearly show that the adhesion features and the growth of LGG biofilms are substrate-dependent.

INTRODUCTION

Bacteria grow preferentially in surface-associated communities called biofilms.[1] The formation of biofilms is a multistage process that includes reversible and irreversible bacterial attachments, the growth of surface-associated colonies, and the release of an extracellular matrix.[2] The strength of the bacterial attachment onto surfaces and the subsequent biofilm growth are affected, among others, by the properties of the supporting substrate. Based on several observations, it was suggested that bacteria interact more strongly with hydrophobic surfaces over hydrophilic ones.[3–5] It was indeed shown for *Staphylococcus epidermidis*, *Pseudomonas aeruginosa*, *Raoultella terrigena*, and *Streptococcus thermophilus* in previous works.[3] Hydrophilic surfaces also showed low adhesive properties for *Listeria monocytogenes*, *Salmonella typhimurium*, *Staphylococcus aureus*, and *Escherichia coli.*[4] Li and Logan studied several bacterial strains on eleven different surfaces, and they found that the number of cells increased with the increase of surface hydrophobic properties for all studied bacterial strains.[5] Besides wetting properties, the charge of the support surface is an important factor in the interplay with bacteria. In physiological conditions, most of bacteria are characterized with an overall negative charge on their cell wall and therefore are electrostatically attracted towards positively charged surfaces.[6] However, the relationship between surfaces and sessile bacteria is not so obvious to predict taking into account only their charges. Indeed, while promoting fast and strong adhesion of bacteria, positive charges may act as biocides and prevent biofilm growth.[7–10]

When administered in adequate amounts, probiotic bacteria are known to confer a health benefit on the host.[11] Hence, the interest in using probiotics in food, medicine and cosmetics supplements has been continuously increasing, which has nowadays resulted in multibillion-dollar industry.[12] To improve industrial and research practices, understanding of their growth on abiotic surfaces is

important, but it is still poorly addressed. Few studies have made evident the ability of probiotics to form biofilms on abiotic substrates such as polystyrene and glass.[13–16] However, for a fundamental understanding of the role of substrate properties in the mechanisms of biofilm development by probiotic bacteria, the control of the physico-chemical properties of the substrate is needed.

A convenient approach to obtain substrates with varying physico-chemical properties is the use of alkanethiol molecules with different functional groups. Grafted on suitable substrates, they provide dense covalently tethered structures with well-defined surface functionality.[17] The possibility to tune the wetting and charge properties of the surface using self-assembled monolayers (SAMs) makes them of great interest to study surface interactions with bacterial biofilms in well-controlled physico-chemical conditions.[18–20] SAMs terminated with $–CH_3$, -OH, and $-NH_2$ functional groups are of particular interest for studying bacterial adhesion, as the former two groups bring to the surface hydrophobic/hydrophilic features, and the latter provides positive charge in physiological aqueous media. For example, the rate of attachment of *Bacillus subtilis* was studied on these model surfaces using surface plasmon resonance (SPR) spectroscopy.[18] Being useful for *in situ* monitoring of the biomass adsorption, SPR spectroscopy is blind to the nature of the adsorbed molecular compounds thus omitting the information on the physiological state of the bacteria that can be affected by the substrate properties. Infrared spectroscopy in attenuated total reflection mode (ATR-FTIR) is a powerful tool, and it is gaining attention in the study biofilms in recent years due to the possibility of monitoring changes in the chemical composition of biofilms in their hydrated state and under different environmental conditions.[21–23] ATR-FTIR spectroscopy requires the use of materials transparent in the infrared spectrum of radiation and possessing a high index of refraction, e.g. zinc selenide or germanium. The feasibility of grafting of alkanethiol SAMs onto

ZnSe was illustrated in the study of Noble-Luginbuhl and Nuzzo.[24] To the best of our knowledge the latter study is the only one to report the results of grafting of alkanethiol SAMs directly onto the ZnSe surface.

Here, the kinetics of self-assembly of alkanethiols onto ZnSe and the organization of SAMs as a function of the terminal group (-CH_3, -OH, or -NH_2) of the alkanethiol chain are investigated. Using these chemically controlled surfaces, the differences in the attachment and the biofilm growth of one of the most commercially utilized probiotic bacterium *Lactobacillus rhamnosus* GG (LGG, a Gram positive rod-shaped bacterium with pili) were demonstrated. The use of an infrared-transparent substrate and its surface control allowed deciphering surface-dependent features in the composition of LGG biofilms and their correlation with changes in the kinetics of biofilm growth in *in situ* measurements. Overall, the substrate functionality played a critical role in the strength of the attachment of LGG biofilms in their nascent and more mature states. The results obtained in this study improve the fundamental understanding of the interaction of LGG with abiotic surfaces and are relevant in the development of research and application strategies of biofilms of probiotic bacteria.

MATERIALS AND METHODS

Materials. A trapezoidal ZnSe ATR crystal (refraction index: 2.4, incidence angle: 45°, Eurolabo, France) that provides six internal reflections on the upper face in contact with the sample was used. 1-Dodecanethiol (≥98%), 11-Mercapto-1-undecanol (97%) and 11-amino-1-undecanthiol hydrochloride (99%) were purchased from Sigma-Aldrich and used as received. Trypticase soy broth (TSB, ref. T8907) was purchased from Fluka (St Louis, MO, USA). Modified TSB (mTSB) medium was composed of 20 $g \cdot l^{-1}$ of Bacto proteose peptone no. 3 (Becton, Dickinson and Co., ref. 211693) and 15 $g \cdot l^{-1}$ of TSB. Ultra-pure water (18.2 MΩ.cm, Elga, Purelab Option-Q) was

used for the rinsing of the crystal, preparation of the physiological saline solution (NaCl 0.9%, pH = 6.0 ± 0.1), and nutritive media for bacteria.

Preparation of functionalized zinc selenide substrates. ZnSe ATR crystals were cleaned with ozone/UV for 15 minutes, rinsed with isopropanol and dried with nitrogen flow.[24] Freshly cleaned crystals were mounted into the infrared flow cell (flow through Gateway ATR top plate from Specac). The mounted infrared cell was filled with a 2 mM ethanolic solution of alkanethiols and left for self-assembly reaction overnight. After the overnight reaction, the surface of the crystal was rinsed inside the cell subsequently with ethanol and sterile ultra-pure water. In separate experiments performed for high-energy elastic backscattering spectrometry and contact angle measurements, the SAMs were obtained on ZnSe disks (Ø 1.8 cm, Crystran, UK) by overnight exposure to alkanethiol solutions followed by the rinse with ethanol and ultra-pure water. The SAMs obtained using 11-amino-1-undecanthiol hydrochloride were additionally rinsed with aqueous physiological saline solution (NaCl 0.9 %) to break a bilayer formed because of hydrogen bonds between amine groups.

***In situ* monitoring of surface functionalization using ATR-FTIR spectroscopy.** The kinetics of the self-assembly process of alkanethiols onto the crystal was monitored using a Bruker Tensor 27 spectrometer equipped with a KBr beam splitter and a deuterated triglycine sulfate (DTGS) thermal detector. Spectra were recorded and processed using the OPUS 7.5 software (Bruker, Karlsruhe, Germany). The spectrum of ethanol recorded just before the start of each experiment was used as a reference. The infrared device was permanently purged with a nitrogen flow to avoid ethanol vapor contribution in the spectra.[25] ATR-FTIR spectra of alkanethiols in ethanol were obtained every 1.5 minutes for the first 45 minutes and then every 20 minutes by recording 100 scans per spectrum at a resolution of 4 cm^{-1}. Water vapor subtraction was performed, and the baseline was

corrected at 3000 and 2780 cm^{-1}. The results presented are representative from three independent experiments.

High-energy elastic backscattering spectrometry. The areal density of alkanethiol SAMs was estimated using high-energy elastic backscattering spectrometry (EBS) measurements with α particles (He^+) by exploiting the non-Rutherford cross-section in the $^{12}C(\alpha,\alpha)^{12}C$ scattering process.[26] The measurements were performed with the 5 MV Cockroft–Walton Tandetron (HVEE B.V., Amersfoort, The Netherlands) at Centro de Micro-Análisis de Materiales (CMAM) from Universidad Autónoma de Madrid. The incident energy of the α projectiles was set at 4265 keV to enhance the sensitivity to C atoms, where the cross-section presents a narrow resonance peak with a value ~20 fold that of the Rutherford one.[26] The incident angle of the beam was 50º to increase the surface sensitivity, whereas backscattered ions were detected at a scattering angle of 170º using a silicon detector. The experimental EBS spectra were analyzed by comparison with simulated spectra in SIMNRA software (Version 7.02)[27]. The results presented are representative from four measurements obtained on two different samples (two spots measured on each surface).

Surface energy measurements. To estimate the surface energy of the functionalized ZnSe, Fowkes theory that dissociates polar and nonpolar (dispersive) components was applied:[28]

$$\frac{\gamma_l(\cos\theta+1)}{2} = \left(\gamma_l^d\right)^{1/2}\left(\gamma_s^d\right)^{1/2} + \left(\gamma_l^p\right)^{1/2}\left(\gamma_s^p\right)^{1/2} \quad (1)$$

where γ_l^d and γ_l^p are the liquid dispersive and polar components, respectively, and γ_s^d and γ_s^p are the solid dispersive and polar components, respectively. First, the contact angle with diiodomethane ($\gamma_l^d = 50.8\ \mathrm{mJ/m^2}, \gamma_l^p = 0\ \mathrm{mJ/m^2}$) was measured, and the dispersive component of the solid surface energy was calculated. Second, ultra-pure water ($\gamma_l^d = 21.8\ \mathrm{mJ/m^2}, \gamma_l^p = 51.0\ \mathrm{mJ/m^2}$) contact angle measurements were performed and the polar component of the solid surface energy

was computed. Fowkes theory assumes that the total surface energy is the sum of the dispersive and polar components: $\gamma_s = \gamma_s^d + \gamma_s^p$ (2)

The measurements of contact angles were performed using a Digidrop contact angle meter (GBX Scientific Instruments). A liquid droplet of 0.5 µL was carefully deposited onto the sample surface with a syringe. The syringe was withdrawn and the image of static contact angle was taken immediately after liquid deposition. The reported contact angle are based on four repeats.

Bacterial strain and preparation of working suspensions. *Lactobacillus rhamnosus* GG (LGG, ATCC 53103) was kindly provided by S. Lebeer (University of Antwerp, Belgium). LGG cultures were prepared as described elsewhere.[29] Briefly, 20 mL and 300 mL of Man-Rogosa-Sharpe medium (ref. 288130, Difco) were used to prepare 24 hours-old subculture and 14 hours-old culture, respectively, at 37°C in static conditions. The working suspensions of LGG were then prepared in 200 mL of physiological saline solution with the resulting optical density of 0.50 ± 0.05 (cell density meter, model 40, Fisher Scientific, Illkirch, France).

Biofilm formation in the infrared flow cell. Freshly prepared LGG working suspensions were put under magnetic stirring (160 rpm) and pumped around a flow cell as previously described,[29,30] over the functionalized ZnSe surface. After the flow cell was filled in with the bacterial suspension, the cells were let to adhere onto the crystal for 30 minutes in static conditions. The flow of the bacterial suspension was then carried out for 2 hours at 50 ml.h^{-1} to obtain 2.5 hours-old biofilms. In separately performed experiments, 1:10 diluted mTSB sterile nutritive medium was flowed over the preliminarily formed 2.5 hours-old biofilm for an additional 24 hours at 50 ml.h^{-1} to allow biofilm growth (hereafter referred to as 26.5 hours-old biofilm).

***In situ* monitoring of biofilm formation using ATR-FTIR spectroscopy.** ATR-FTIR spectra were recorded every 10 minutes for the first 2.5 hours of the experiment, and every 20 minutes

during the period of the flow of the sterile 1:10 mTSB (24 hours), to monitor *in situ* the attachment and growth of bacteria on the functionalized ZnSe. The spectrum of the bacterial suspension obtained immediately after filling in the flow cell was used as a reference for the spectra obtained during the first 2.5 hours of the measurements. The spectrum of the sterile 1:10 mTSB obtained once it had replaced the bacterial suspension was used as reference for the spectra recorded during the flow of 1:10 mTSB over preliminarily attached cells for 24 hours. Water vapor subtraction was performed and the baseline was corrected at 1800 and 900 cm^{-1}. All experiments were conducted at 21±1°C in an air-conditioned room.

Epifluorescence microscopy. *Bac*Light™ Live/Dead kit (Molecular Probes, ref. L7012) was used to stain bacterial cells. This kit contains two fluorochromes, green-fluorescent Syto 9 and red-fluorescent propidium iodide, which enable determination of the permeability state of the cell membrane. Syto 9 is able to penetrate into all cells, whereas propidium iodide enters only the cells with compromised membranes making damaged bacteria to appear red. Once 2.5 and 26 hours-old biofilms were formed, the ATR crystal was carefully demounted from the flow cell and gently dipped into the Petri dish filled with sterile ultra-pure water. Bacteria on the crystal surface were then stained with the *Bac*Light™ kit for 20 minutes in the dark at 21±1 °C. The crystal was then gently dipped into a Petri dish filled with sterile ultra-pure water to eliminate excess dyes. A series of images (≥60) was recorded along the crystal surface using ×10 objective of an Olympus BX51 microscope. The images were processed with the ImageJ software for the calculation of bacterial coverage on the crystal surface.

In situ monitoring of bacterial detachment using a flow of nitrogen bubbles. A continuous flow of nitrogen bubbles (volume ~0.2 cm^3, ~15 bubbles per minute) in physiological saline solution at 15 mL/min was carried out over the cells attached during the preliminary flow of the

bacteria suspended in physiological saline solution for 2.5 hours in the infrared flow cell. The detachment of the cells as a result of the passage of the nitrogen bubbles was monitored *in situ* by recording ATR-FTIR spectra for 3.5 hours. The experiments were conducted at 21±1°C in an air-conditioned room. The spectra were processed as described above for the spectra recorded during the period of biofilms formation.

Atomic force spectroscopy. To study the interaction of the LGG cell wall with -CH_3, -OH, and -NH_2 functional groups, adhesion forces between functionalized AFM probes and the LGG cell wall were carried out. The experiments were performed at 21±1°C in liquid medium using a MFP-3D-BIO atomic force microscope (Oxford Instruments, Santa Barbara, CA, USA) equipped with a cell that was filled with 2.5 mL phosphate buffered saline (pH 6.8). Gold-coated AFM probes (NPG-10, Bruker) were functionalized with alkanethiols $HS(CH_2)_{11}X$ (X=CH_3, OH, or NH_2) by exposure to 1 mM ethanolic solution of the corresponding alkanethiol. LGG cells at exponential growth phase suspended in phosphate buffered saline were immobilized (14 hours, 4°C) through electrostatic interactions with $–NH_3^+$ terminal groups of SAM of 11-Amino-1-undecanethiol adsorbed onto Au/Cr/glass (Sputter Q150T, Quorum technologies).[31] The interactions between the functionalized probes and the LGG cell wall were quantified by scanning the surface and measuring the deflection of the cantilever as a function of the vertical displacement of the piezoelectric scanner. A total number of 1024 force-distance curves were recorded on the sample spot with the size of 100 μm^2. These curves were analyzed using a custom program in MATLAB software for calculation of the frequency of appearance of an interaction force as a function of the probe-sample distance.

RESULTS

Functionalization of ZnSe with alkanethiols and characterization of the obtained surfaces. The functionalization of the surface with three different alkanethiols was performed on the ZnSe crystal mounted into the infrared cell, and the process of thiol adsorption onto the surface was monitored *in situ* using ATR-FTIR spectroscopy. Hereafter, the SAMs obtained on ZnSe using 1-dodecanethiol, 11-mercapto-1-undecanol, and 11-amino-1-undecanthiol hydrochloride are referred to as SAM-CH_3, SAM-OH and SAM-NH_2, respectively. Figure 1 shows the ATR-FTIR spectra recorded during the self-assembly reaction from the alkanethiol solutions. The increase of νCH_2 bands indicated the adsorption of thiol molecules onto the surface.

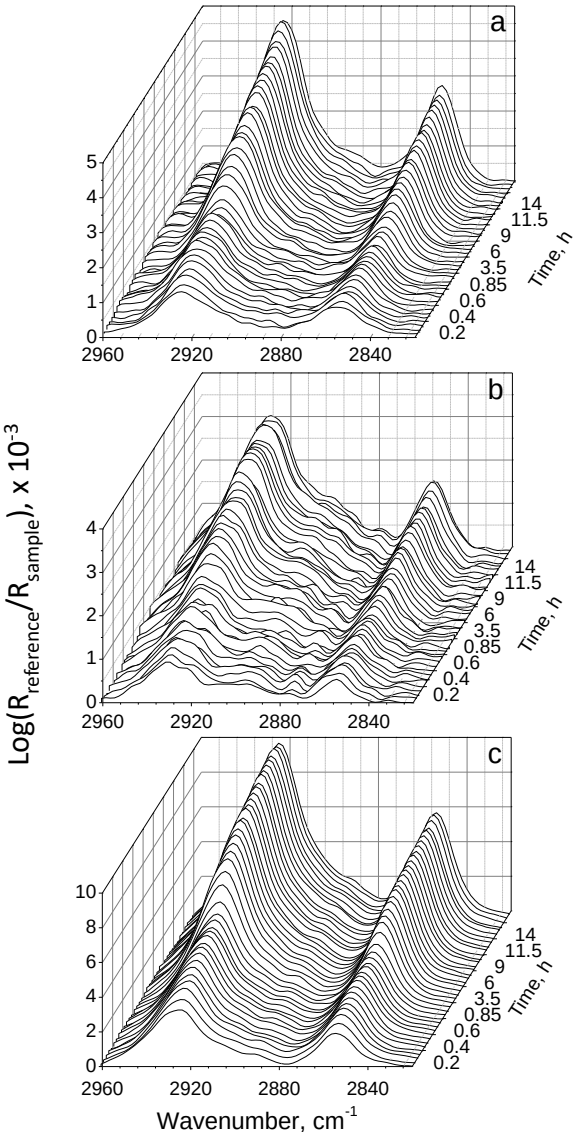

Figure 1. Time-evolution ATR-FTIR spectra depicting νCH_2 bands of alkanethiol molecules terminated with CH_3 (a), OH (b), and NH_2 (c) groups, in ethanolic solution. The spectrum of ethanol recorded immediately before the inflow of alkanethiol solution served as a reference.

Interestingly, the wavenumbers of these bands were varying as a function of time and with respect to the terminal group of the alkanethiol molecules (Table 1). The wavenumber of $\nu_{asym}CH_2$ band provides insight into the intermolecular environment of the alkyl chains.[32] Lower frequencies of

vibrations indicate a lower number of conformational defects, whereas the wavenumber at ~2918 cm^{-1} is considered representative for crystalline-like structure. From the decrease of the wavenumber for $\nu_{asym}CH_2$ band from the beginning to the end of the monitoring of the assembly process, all studied alkanethiols increased the degree of ordering in SAMs with time (Table 1). Moreover, it can be noticed that the SAM-OH had the least ordered organization, as this value was 3 cm^{-1} higher than for the other two SAMs after 16 hours of reaction.

Table 1. Wavenumbers of νCH_2 antisymmetric and symmetric bands for alkanethiols with different functional groups at the beginning and at the end of the reaction

	SAM-CH_3		**SAM-OH**		**SAM-NH_2**	
	$\nu_{asym}CH_2$	$\nu_{sym}CH_2$	$\nu_{asym}CH_2$	$\nu_{sym}CH_2$	$\nu_{asym}CH_2$	$\nu_{sym}CH_2$
~2 min	2927	2855	2929	2855	2926	2854
~16 hours	2924	2853	2927	2854	2924	2853

The low degree of the organization in SAMs is usually associated with less packed monolayers. To compare the surface coverage with SAMs as a function of the terminal group, the intensities of $\nu_{sym}CH_2$ band in the spectra recorded over time of the reaction were integrated, and the values obtained were used as indicators of the kinetics of the reaction process (Figure 2a). As estimated from these integrated intensities, the surface coverage was in the order SAM-NH_2 > SAM-CH_3 > SAM-OH. In particular, 2.8 and 5.8 fold higher integrated intensities were observed at the end of the measurements and before ultra-pure water rinse for SAM-NH_2 compared to SAM-CH_3 and SAM-OH, respectively. Here, it must be noted that amino-terminated SAMs tend to form a bilayer

due to hydrogen bonding.[33,34] The bilayer contribution into the spectrum intensity in the case of SAM-NH_2 can be estimated after the rinse with ultra-pure water based on the signal intensity decrease (Figure 2b). It is also noteworthy that, after the rinse, $\nu_{asym}CH_2$ band has slightly shifted (≈1 cm^{-1}) to the lower wavenumber indicating a small increase in the organization of SAM-NH_2 after breaking the bilayer (Figure 2b).

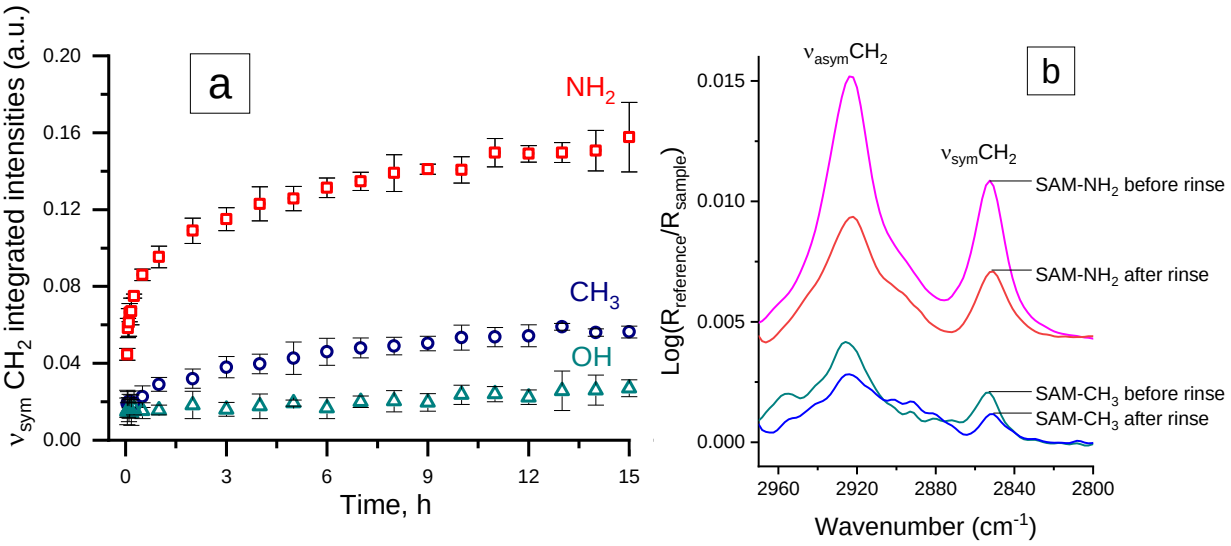

Figure 2. (a) Time evolution of the integrated intensities of $\nu_{sym}CH_2$ band (2874–2814 cm^{-1}) of alkanethiol SAMs terminated with amine (NH_2), methyl (CH_3) and hydroxyl (OH) groups. a.u.: arbitrary units. Error bars represent standard deviations from three measurements. (b) ATR-FTIR spectra depicting νCH_2 bands of amino- and methyl-terminated SAMs at the end of the overnight reaction before and after rinse with ethanol and ultra-pure water. The area marked is the integrated intensity of $\nu_{sym}CH_2$ band. The reference spectrum is the spectrum of ethanol recorded immediately before the inflow of alkanethiol solution in the infrared flow cell. Offsets of spectra are used for clarity.

In the case of SAM-OH, the formation of a bilayer can also be expected via hydrogen bonds. However, it was earlier demonstrated by te Riet *et al.* that SAM-OH did not appear to form interlayer hydrogen bonds.[33] As suggested by these authors, this result could be explained by an unfavorable competition with the formation of strong hydrogen bonds between the molecules within the SAM-OH, or an unfavorable competition with the solvent for hydrogen bonding. Based on these findings and from our observations of the low intensities obtained for SAM-OH (Figure 2a), the organization of SAM-OH was represented by a monolayer on ZnSe. However, the scenario in which the low intensity is obtained as a result of very low packing density of the monolayer and some hydrogen-bonded molecules lying on top of it cannot be excluded. The definitive conclusion on the possible bilayer formation for SAM-OH is complicated by the fact that the intensities obtained were very low. For SAM-CH_3, the decrease in the intensity of the spectrum obtained after the rinse indicated a possible contribution of physically adsorbed molecules into the spectra preliminarily the rinse (Figure 2b).

To elucidate further the difference in surface coverages between SAMs, EBS measurements were performed. The overall EBS spectrum represents a superposition of the signal from each individual element. The detected energy of the backscattered projectiles increases and decreases with the recoil mass and the collision depth, respectively. This implies that the energy extension for each element provides information about the corresponding *in depth* distribution. Moreover, the relative yield for each element is proportional to its atomic concentration weighted by the corresponding scattering cross-section. The Rutherford scattering cross-section for light elements is relatively low, so the enhanced sensitivity for carbon in EBS provides a more reliable quantification. In particular, this method was successfully applied earlier to study the surface coverage with alkanethiol SAMs based on the signal from carbon.[26] Figure 3 shows EBS spectra of alkanethiol SAMs terminated

with CH_3, OH, and NH_2 groups. Despite the relatively low amount of carbon in the sample (surface monolayer), a prominent signal can be detected lying atop of the strong signal from the heavier elements of the ZnSe substrate. The insert in Figure 3 depicts the difference in carbon counts for the three different SAMs. The highest signal was observed in case of the SAM terminated with the amine group.

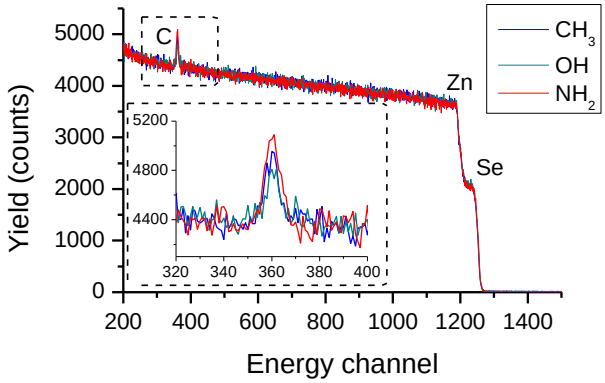

Figure 3. EBS spectra of alkanethiol SAMs terminated with CH_3, OH, and NH_2 groups

Furthermore, as shown in Table 2, the results of EBS measurements on carbon coverage indicated that the surface coverage with alkanethiol molecules was 1.6- and 1.7-fold higher in SAM-NH_2 than in SAM-CH_3 and SAM-OH, respectively. The values of coverages obtained with EBS were in good agreement with the results obtained from ATR-FTIR spectra after the rinsing step (Figure 2b).

Table 2. Surface coverage with SAMs and surface energy of the functionalized substrates

		SAM-CH_3	**SAM-OH**	**SAM-NH_2**
Carbon coverage	atoms/nm^2	52 ± 5	45 ± 5	75 ± 5
	molecules/nm^2	4.3 ± 0.5	4.0 ± 0.5	6.8 ± 0.5

Contact angle H_2O	89.8 ± 0.5	70.4 ± 2.1	68.5 ± 3.3
Contact angle CH_2I_2	40.1 ± 1.5	35.0 ± 0.3	41.0 ± 1.3
Surface energy, mN/m	40.6 ± 0.7	48.7 ± 0.9	47.4 ± 0.8

Ultra-pure water contact angles measured in this work (Table 2) are in good agreement with those of Noble-Luginbuhl and Nuzzo.[24] For the SAM-NH_2, the values obtained here were somewhat higher than those expected from literature on SAMs formed on gold (~40–50°).[35–37] This can be attributed to the lower degree of ordering in SAMs obtained on ZnSe than on Au and, hence, more methylene groups at the outmost surface of SAMs onto ZnSe, which lead to a lower hydrophilic character of the surface. For SAM-OH, the values usually reported are below 30°.[35,37] Since SAM-OH obtained in the present study was with defects in the structure, it could result in the inclining of the alkanethiol chains and looser structure. The water contact angle measured on SAM-OH is in accordance with the value reported for loosely packed hydroxyl-terminated alkanethiol SAMs on gold (≈68°).[38] In addition, the higher roughness of ZnSe compared to gold-coated glass can contribute to a loose structure of SAM-OH and consequently low wetting properties of this SAM. In the perspective of the study of bacterial attachment, the surface energy of functionalized substrates was determined based on the contact angle measurements with utra-pure water and diiodomethane (Table 2). The data showed that the SAM-CH_3 led to the surface with the lowest energy value, as expected from the lack of the polar groups, whereas the values obtained on surfaces with SAM-NH_2 and SAM-OH were similar to each other.

Spectral fingerprint and initial attachment of LGG cells as a function of the substrate functional groups. In the aqueous media used, functionalization of the substrates provided

hydrophobic non-charged (SAM-CH_3), hydrophilic non-charged (SAM-OH) and hydrophilic positively charged (hereafter called SAM-NH_3^+)[35] surfaces. Once these surfaces were characterized, they were subjected to a flow of LGG suspended in physiological saline solution for 2.5 hours (30 minutes at static mode and 2 hours under flow). The kinetics of LGG adhesion to the substrates was monitored based on the increase of amide II band intensities during the inoculation of LGG suspension (Figure 4). The use of this band as an indicator for biomass quantity is justified by the fact that proteins are the most abundant molecules in bacterial cells, and a positive correlation between amide II band and biomass quantity was already reported.[39,40] It must be noted that the obtained curves represent primarily the lateral increase of the biomass amount, since the sampling depth is only within 1-2 µm above the substrate. The increase of amide II band was very close on the substrates with SAM-CH_3 and SAM-OH, whereas on SAM-NH_3^+ it was faster with higher obtained values for the integrated intensities (0.8, 0.7 and 0.7 for SAM-NH_3^+, SAM-CH_3 and SAM-OH, respectively) after 2.5 hours of bacterial flow. According to Kang *et al.*[41], the kinetics of bacterial attachment can fit the following equation:

$$A = A_{max}(1 - e^{-kt}) \quad (3)$$

where A_{max} is the amide II band integrated intensity corresponding to a complete single layer of bacteria, k is the rate constant, and t is the time of bacterial exposure. It is important to note that, besides the suspension concentration, such an adsorption rate constant is dependent on the accessory optics. Therefore, the results can be compared only with those obtained using the same ATR-FTIR device. The results corresponding to LGG attachment onto the three functionalized substrates fit well this model of adsorption (regression coefficient $r^2 > 0.99$ for all curves, Figure 4). The rate constant values were 0.64, 0.86, and 0.99 h^{-1} for LGG attachment on ZnSe

functionalized with CH_3, OH and NH_3^+ groups, respectively. Thus, the highest rate of LGG attachment was observed onto the amino-terminated surface.

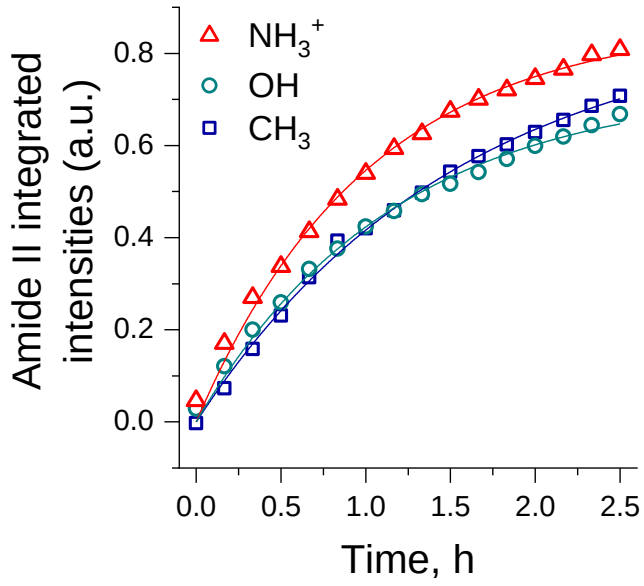

Figure 4. Time-evolution of amide II band integrated intensities (1592-1486 cm^{-1}) during the exposure of LGG suspension over ZnSe functionalized with alkanethiol SAM terminated by CH_3, OH or NH_3^+ functional groups. The curves were fitted using equation (3)

The ATR-FTIR spectra obtained after 2.5 hours of LGG exposure on the substrates with SAM-CH_3, SAM-OH, and SAM-NH_3^+ are shown in Figure 5a. The close intensities of the obtained spectra showed that LGG was able to attach onto substrates regardless of their functionalization properties. The spectral features were overall similar on all studied substrates resembling common biochemical components of bacterial cells, i.e. proteins, nucleic acids (NA), phospholipids (PL) and polysaccharides (PS).[29,42] Nonetheless, a slight difference can be noticed for νC=O (~1710 cm^{-1}) and νCOO^- (~1415 cm^{-1}) bands, which were more intense on NH_3^+-functionalized substrate. These bands were assigned to carboxylic functions, which could be specifically linked to NH_3^+ moieties of the surface. The analysis of the ratios of main components of bacterial cells (Figure 5b)

suggests that the ratio of nucleic acids and phospholipids to a sum of nucleic acids, phospholipids and polysaccharides (NA+PL / NA+PL+PS) was similar regardless of the substrate. At the same time, the protein content was higher with respect to nucleic acids, phospholipids and polysaccharides (Amide II / NA+PL, Amide II / NA+PL+PS) on the substrate with SAM-NH_3^+. Therefore, based on the calculated ratios it can be suggested that the higher intensities of νC=O and νCOO^- bands on the surface with SAM-NH_3^+ (Figure 5a) were due to the higher interaction of the peptidic moieties from the peptidoglycan layer with NH_3^+ groups.

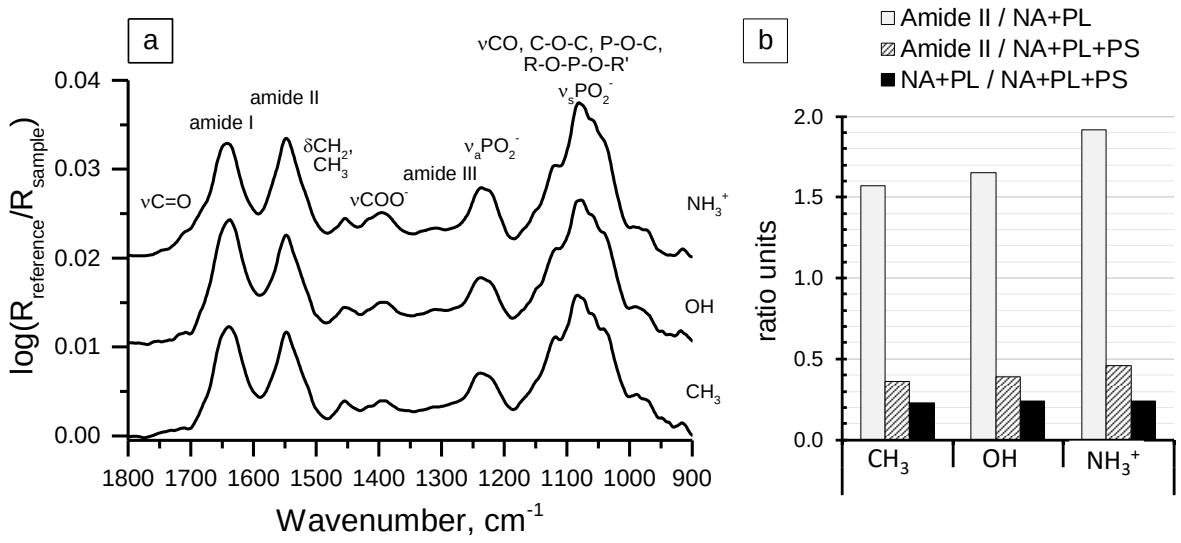

Figure 5. (a) ATR-FTIR spectra of LGG suspended in physiological saline solution after 2.5 hours of exposure on ZnSe functionalized with alkanethiol SAMs terminated with -CH_3, -OH, and -NH_3^+ groups. Offsets are used for clarity. NA – nucleic acids, PL – phospholipids, PS – polysaccharides. The reference spectrum was obtained immediately after filling in the infrared flow cell with LGG suspension. (b) Ratios of integrated intensities of bands corresponding to proteins (amide II, 1592 –1486 cm^{-1}), NA + PL (1271–1188 cm^{-1}), and a combination of NA, PL and PS (1189–956 cm^{-1}).

The amide II band was used for proteins estimation, as it has little interference with the signal for δH_2O at 1640 cm^{-1}.

Degree of retention of LGG and membrane integrity on the functionalized substrates. After inoculation of the bacterial suspension for 2.5 hours, the crystal was extracted from the flow cell, and the bacteria on the surface were stained using the *Bac*Light™ kit after a gentle rinse. The retention of cells on the substrates after the rinsing step was strongly substrate dependent (Figure 6). The retention was very poor on CH_3- and OH-terminated substrates, whereas on NH_3^+-terminated substrate the cells retained and they were homogeneously spread on the crystal. The chain-like pattern observed on the latter substrate (Figure 6c) can be associated with the presence of pili on the LGG cell wall.[43] A similar chain-like pattern of bacterial distribution at surfaces was shown earlier for LGG,[44] and other lactobacilli.[16]

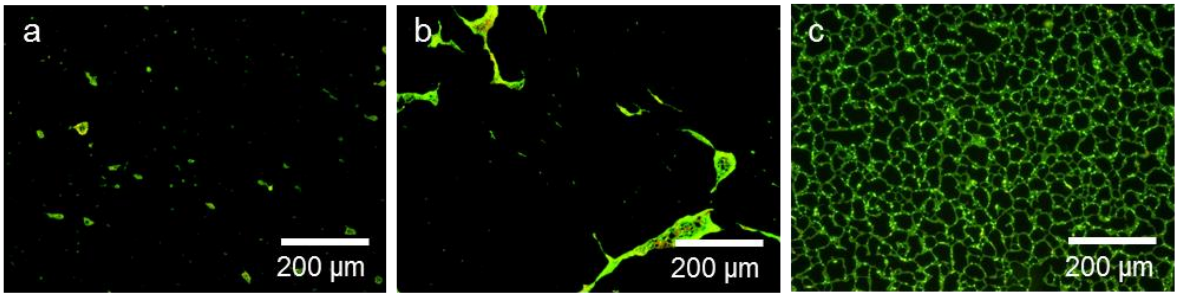

Figure 6. Epifluorescence images (*Bac*Light™ staining) presenting LGG cells after 2.5 hours exposure on the substrates functionalized with SAM-CH_3 (a), SAM-OH (b), and SAM-NH_3^+ (c).

As the bacterial distribution on the surfaces with SAM-CH_3 and SAM-OH were drastically affected by the rinsing step (i.e., movement and dislocation of bacterial cells during rinsing), the pristine estimation of the effect of these functional groups on the membrane integrity of the cells was complicated on these surfaces. In addition, there was a very low number of cells on these substrates (~0.5% average coverage on SAM-CH_3 and ~7% average coverage on SAM-OH), and many of

them were gathered in overlaying patches. On the surface with SAM-NH_3^+, the cells appeared green indicating the integrity of their membrane.

Impact of the surface functionalization on the interaction with LGG. The results presented above showed that LGG appeared to attach on all studied substrates in the infrared flow cells but did not respond in the same manner to a rinsing step. To illustrate further the effect of the substrate on LGG stability onto the surface, it was attempted to evaluate the detachment of bacterial cells *in situ* in the infrared flow cell based on variations of signal intensity under induced mechanical stress. It was suggested that the force arising at the air-liquid interface, when this interface is in contact with the bacterial cell (as in the rinsing step), is a determining factor in the detachment of bacteria from the substrates.[45] To check this hypothesis, an experiment using a continuous flow of nitrogen bubbles in physiological saline solution was set up, in which the effect of these bubbles on the attached bacteria was monitored *in situ* in the infrared flow cell. Figure 7 presents the time evolution of amide II band integrated intensities during bubbles flowing over LGG cells attached on the three different substrates.

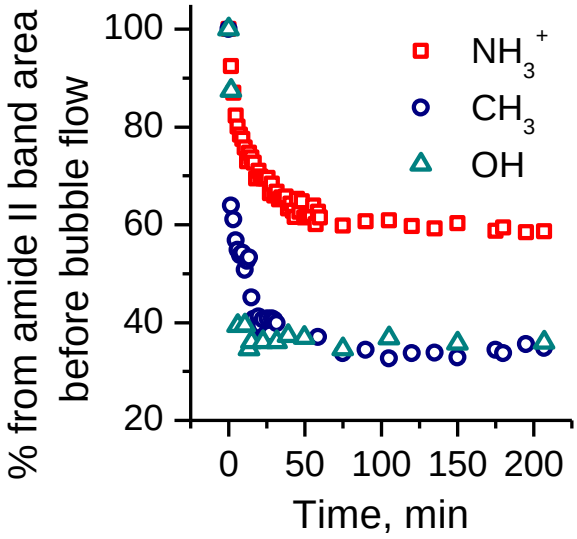

Figure 7. Time-evolution of amide II band integrated intensity during nitrogen bubble flowing over LGG cells after 2.5 hour of preliminary exposure on substrates functionalized with alkanethiol molecules terminated with CH_3, OH and NH_3^+ groups

The sharp decrease in amide II band integrated intensity suggested the removal of cells from the substrates under the mechanical stress applied. This removal occurred faster and to a higher extent on the SAM-CH_3 and SAM-OH substrates. Similar observations of bacterial removal from surfaces as a result of the passage of air bubbles were reported previously.[3,46] As it can be seen in Figure 7, the integrated intensities reached a pseudo-plateau after ~1 hour, and then stayed constant for the following 2.5 hours of measurements on all substrates. The highest value of amide II integrated intensity after continuous flow of bubbles was observed on the substrate with SAM-NH_3^+. It must be noted that the lifting force arising at the passage of an air bubble is dependent on the substrate functional properties.[3] The lifting force was calculated up to five time higher on a hydrophobic surface (i.e. with a low surface energy) than on a hydrophilic surface (i.e. with a high surface energy),[3] and the same trend was expected here. Therefore, the conclusion on the magnitude of the interaction forces between LGG and the functionalized substrates cannot be made based on the measurements of the nitrogen-bubble-induced bacterial detachment.

To obtain the information on the interaction forces between LGG cells and the three functional groups (-CH_3, -OH, -NH_3^+), atomic force spectroscopy was then performed. The immobilized bacteria were intermittently approached with AFM probes functionalized with -CH_3, -OH or -NH_3^+ terminated alkanethiol molecules. The force curves of the interaction between LGG and the functionalized probes were then recorded and analyzed using custom MATLAB software. The adhesion forces that have occurred at various rupture distances between LGG and alkanethiol molecules with different terminal groups were extracted from the force curves, examples of which

are presented in Figure 8a,c,e, and plotted as maps depicting the probability of adhesive events (Figure 8b,d,f).

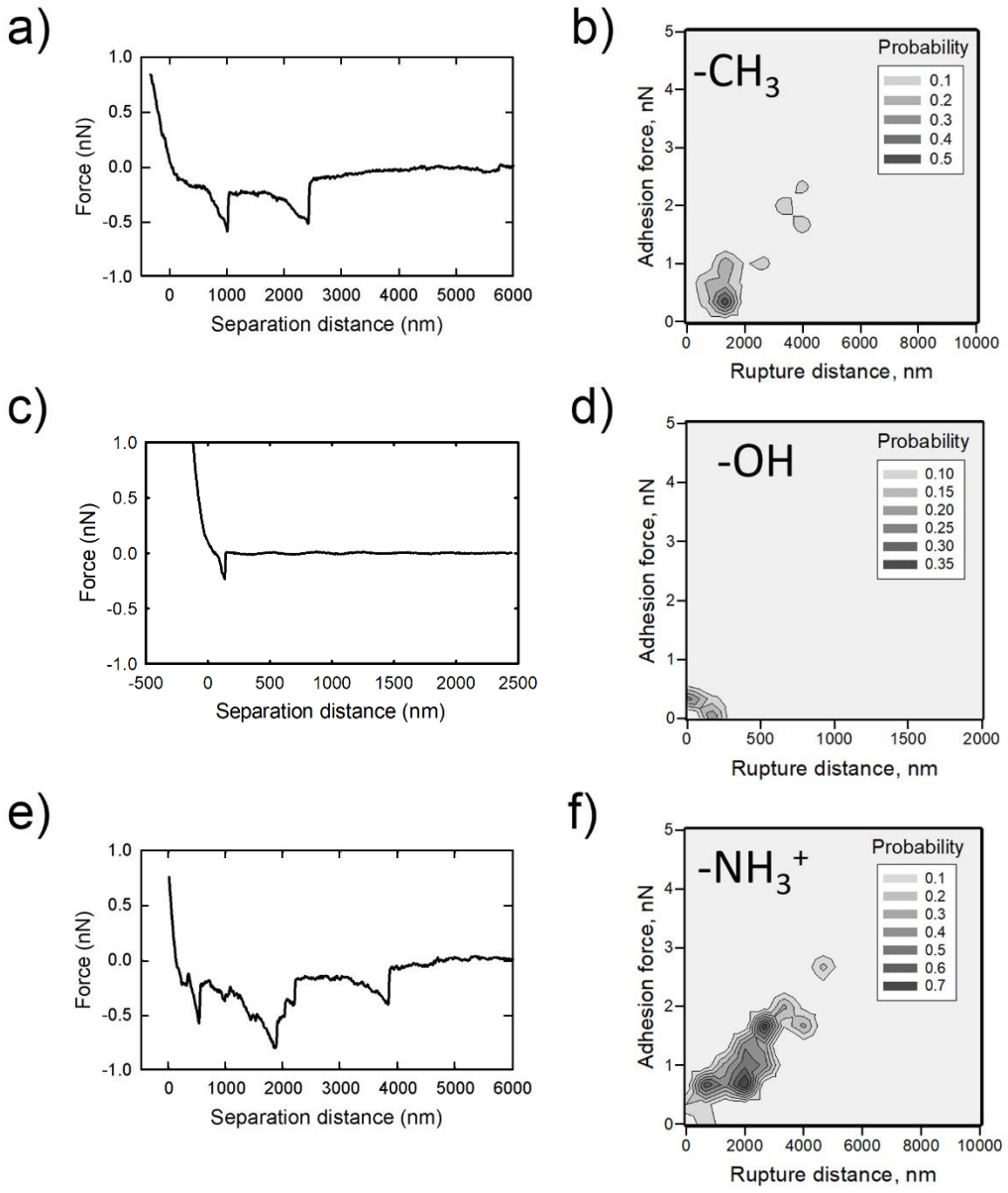

Figure 8. Representative force curves (a, c, e) and force-distance maps (b, d, f) for the interactions between the LGG cell wall and the AFM probe functionalized with alkanethiols terminated by CH_3 (a, b), OH (c, d), or NH_3^+ (e, f) groups recorded in phosphate buffered saline

The rupture distance here represents the longest distance at which the interaction between the probe and the wall of the bacterial cell still occurs as the probe retracts upwards from the sample surface. The interaction was the weakest between LGG and -OH functional group, reaching maximum 0.5 nN at the rupture distance of 250 nm (Figure 8c,d). The adhesive forces between the $-CH_3$ group and LGG were spread in a larger spectrum of values (more frequently being around 0.3 nN with rare events at ≈2 nN) and occurring at longer rupture distances (mostly between 1 and 2 μm, but present up to 4 μm) (Figure 8a,b). Higher adhesive forces at longer rupture distances between LGG and $–CH_3$ group with respect to –OH, can be due to unfolding and stretching of proteins that expose fresh hydrophobic groups for the interaction.[47] The highest interaction forces at longer rupture distances were found between LGG and $-NH_3^+$ group: high probability interactions were between 0.5 and 2 nN, reaching up to 2.5–3 nN at rupture distances up to 5 μm (Figure 8e,f). The strongest interaction forces observed between LGG and the amino-functionalized AFM probe were in good agreement with the results obtained with ATR-FTIR spectroscopy and epifluorescence microscopy.

24 hours development of LGG biofilms on functionalized substrates. The growth and membrane integrity of LGG cells on two selected substrates (SAM-NH_3^+ and SAM-CH_3) were studied in a long-term experiment in order to find out how important the substrate functionality is in the maturation process of the biofilm and the stability of the biofilm on the surface. Figure 9 shows the evolution of ATR-FTIR spectra depicting LGG biofilm formation as a function of the time on both substrates in 1:10 mTSB. Second derivatives calculated at specific times for deciphering spectral features are also presented in Figure 9.

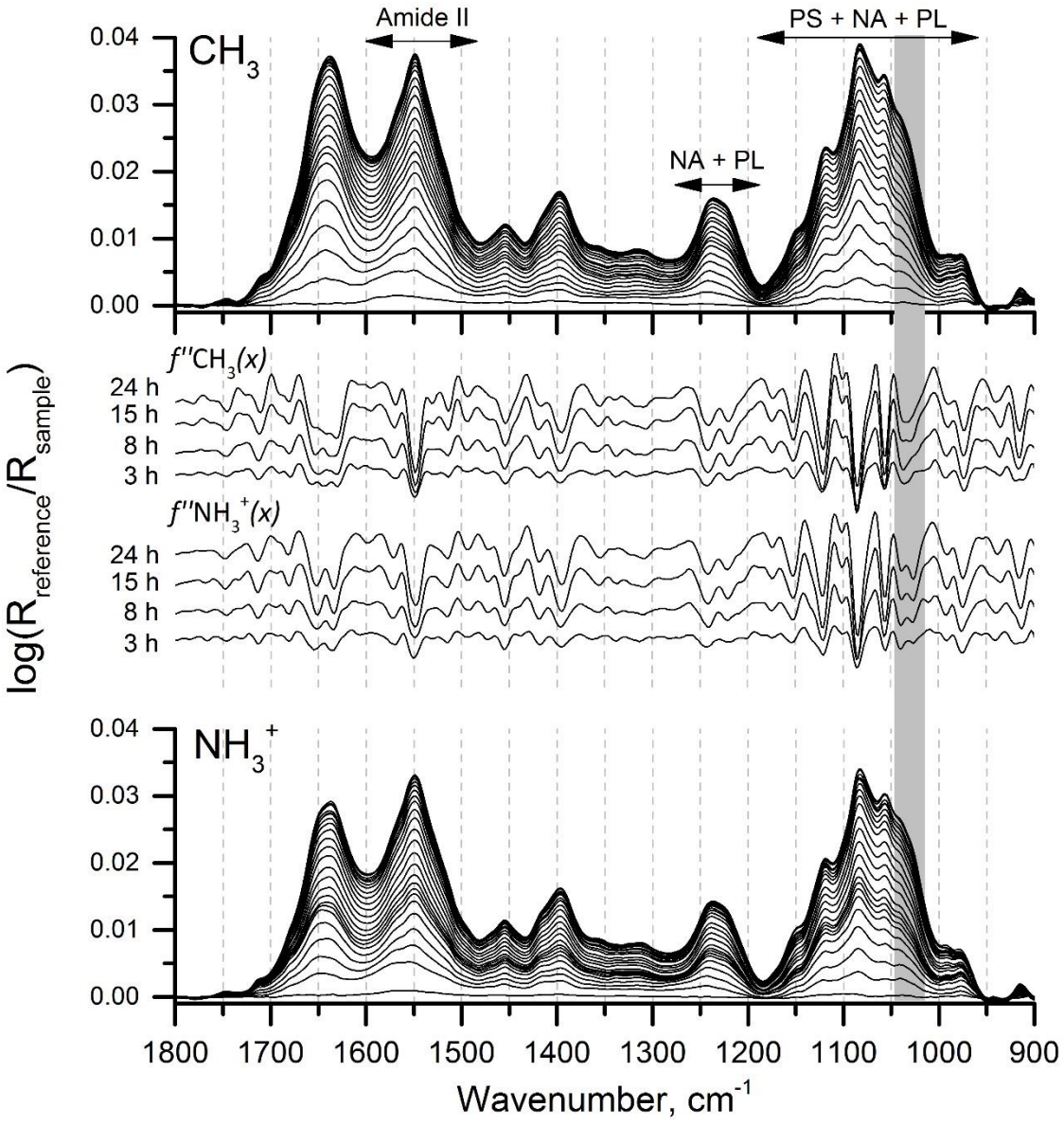

Figure 9. Time-evolution of ATR-FTIR spectra during 24 hours of LGG biofilm development in 10-fold diluted mTSB medium on $-CH_3$ and $-NH_3^+$ functionalized substrates (1 hour interval). Middle panel: second derivative f″(x) of the spectra recorded at 3, 8, 15 and 24 hours. The reference spectrum is the spectrum obtained immediately after the nutritive medium had replaced bacteria suspended in physiological saline solution preliminarily inoculated for 2.5 h hours. Key for bands

assignment: NA+PL = nucleic acids + phospholipids, and PS = polysaccharides. The bands around 1030 cm^{-1} are marked grey to emphasize the difference in polysaccharide bands.

The general look of the spectra and their evolution with time were similar on both substrates. This suggests that the substrate functionality did not drastically affect the biochemical composition of LGG biofilm and the ability of LGG to grow into a biofilm. Nonetheless, the features obtained in the second derivative spectra revealed an apparent difference in the polysaccharides bands around 1030 cm^{-1} (Figure 9). This difference was present already after 3 hours of bacterial growth on the surfaces, and it was more pronounced with time. The lack of change in other bands in the spectra of LGG obtained on two different surfaces did not allow a conclusion regarding the possible nature of the polysaccharides synthetized by LGG on the SAM-NH_3^+ substrate (i.e., the characteristic band at 1026 cm^{-1}). It can be hypothesized that the physiological activity of LGG was switched to produce specific polysaccharides in order to adapt to strong electrostatic interactions induced by a positively charged SAM-NH_3^+ substrate. This hypothesis, as well as the specific composition of polysaccharides synthetized by LGG in the biofilm as a function of the substrate, would be of great interest to address in future studies.

Furthermore, to estimate the difference in the kinetics of the growth of LGG biofilm on the two substrates the integrated intensities of main bands marked in Figure 9 were calculated as a function of time (Figure 10). On the substrate with SAM-CH_3, the integrated intensities of all studied band regions increased steadily until a plateau was reached after ~15 hours of the nutritive medium flow over LGG cells (Figure 10a). Surprisingly, on the substrate with SAM-NH_3^+, the kinetics of integrated intensities was not following the same trend. Indeed, the bands were increasing with the similar rate compared to -CH_3 terminated substrate for the first 6 hours, but afterward, the growth was slowed down for ~2 hours (Figure 10b). Subsequently, LGG increased the rate of its growth

until ~15th hour on the surface. Based on the aforementioned difference in polysaccharides synthetized by LGG on SAM-NH_3^+ and SAM-CH_3, the slowing down of bacterial growth on SAM-NH_3^+ substrate may be seen as a change in physiological activity of LGG to produce specific polysaccharides for an adaptation of growth on the strongly adhesive positively charged substrate.

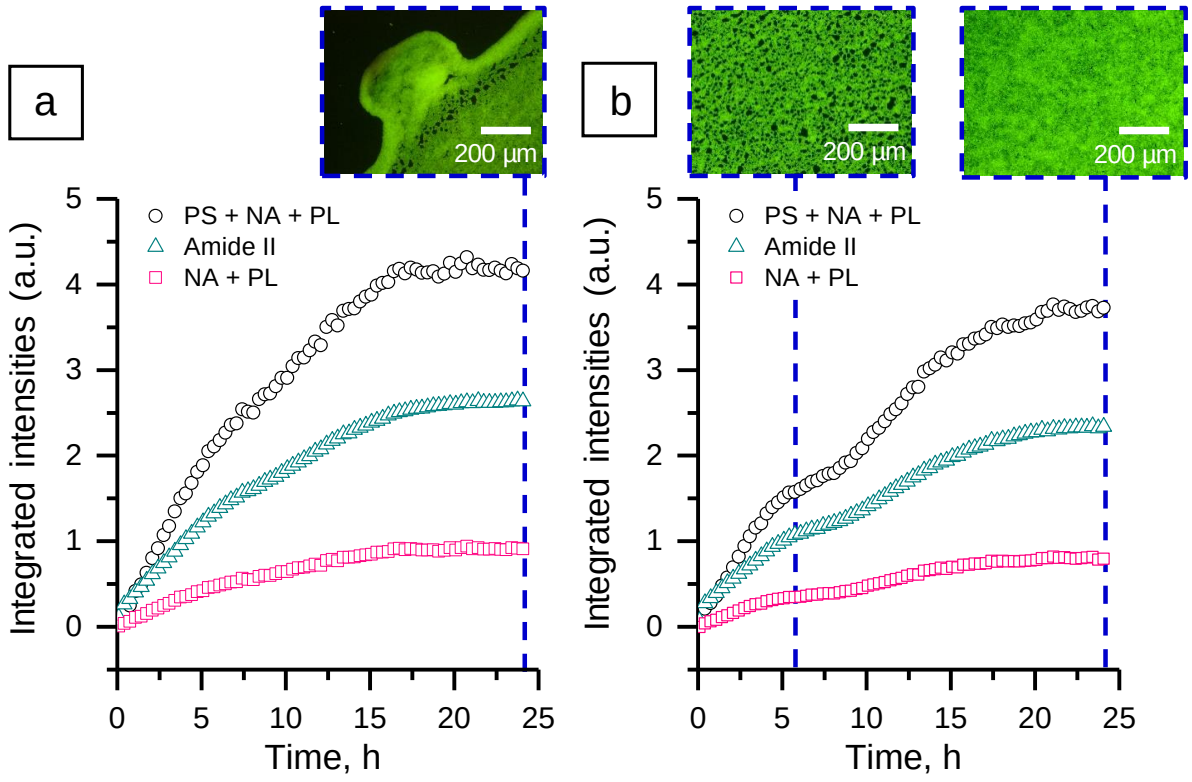

Figure 10. Evolution of integrated intensities of the ATR-FTIR bands corresponding to proteins, as derived from the amide II band (1592–1486 cm^{-1}), nucleic acids + phospholipids (NA + PL, 1271–1188 cm^{-1}), and polysaccharides + nucleic acids + phospholipids (PS + NA + PL, 1189–956 cm^{-1}) during the formation of LGG biofilm for 24 hours in 1:10 mTSB on -CH_3 functionalized (a) and -NH_3^+ functionalized (b) substrates after initial 2.5 hours of bacterial flow in physiological saline solution. Inserts: epifluorescence images of LGG cells after staining with the *Bac*light^{TM} kit after 6 (b) and 24 (a, b) hours of the flow of the sterile nutritive medium. a.u.: arbitrary units.

The distribution of the cells on the substrates functionalized with SAM-CH_3 and SAM-NH_3^+ was different after 24 hours of the exposure of LGG cells and substrate rinse. On the -CH_3 functionalized substrate, some parts of the crystal were fully covered with bacterial cells, whereas others were completely empty. The epifluorescence image in Figure 10a shows an example of the border between the part of the crystal fully covered with bacteria and the empty part. From the observations of the crystal surface during the rinsing step, it was concluded that the biofilm initially present at the crystal surface tends to be lifted by rinsing and/or staining solutions. Indeed, the lifting force arising at the interface between bacterium, liquid and air is especially high on hydrophobic surfaces.[46,48] On the substrate functionalized with SAM-NH_3^+, bacteria developed gradually into a biofilm eventually providing fully covered surface (average coverage >90 %). The bacteria appeared green showing an intact membrane in the conditions of growth on this substrate (Figure 10b).

DISCUSSION

Substrates with well-defined surface chemistry are important for understanding the process of bacterial attachment and biofilm development. Their precise characterization is necessary for extracting a reliable correlation between surface properties and bacterial fate. In this study, we used ZnSe crystals functionalized with three different alkanethiol molecules that possess either methyl, hydroxyl or amine functional groups. After rinsing, a small difference between the surface coverage with SAMs was observed depending on the terminal group of the alkanethiol molecule. Amino-terminated alkanethiols formed the densest SAMs. The coverage was 1.5 fold higher than the one expected for the well-ordered SAM on the atomically flat gold surface (4.5 molecules/nm^2).[49] This difference may be a consequence of the high surface area of the relatively rough ZnSe substrate.[24] In the case of SAM-CH_3 and SAM-OH, the found areal density was lower, and our data indicate a

lower degree of molecular organization for these SAMs with respect to SAM-NH_2. The low organization of SAM-OH has been earlier demonstrated on atomically flat gold surfaces.[50] As the authors suggested, this could be reasoned by the terminal group size. The definitive nature of the defects in SAM-OH seem not to be clear, but they were also observed in studies with gold,[50] and gallium arsenide.[51]

As expected, the surface energy of the substrates also varied as a function of the terminal group of alkanethiol molecules in SAMs. The surface energies found in this work are difficult to compare with those reported in literature due to the differences in models used for the calculation and applied solvents.[52] Nonetheless, the surface energies calculated for SAM-NH_2 and SAM-OH were very close and this parameter cannot explain alone the difference of retention of LGG on both surfaces. The results obtained by multiple approaches in the present work put in evidence several important factors regarding the role of substrate functionality in LGG attachment and growth. LGG attaches quicker on positively charged substrates than on hydroxyl and hydrophobic ones. Overall, this result is in accordance with other works demonstrating faster adhesion rates of different bacterial species on SAMs terminated with amine groups.[19,36,53] Furthermore, it has been claimed that bacterial cells attach preferentially to hydrophobic materials (materials with low surface energy) due (i) to a mismatch between their surface energy and a typically higher surface energy of liquids in which cells are suspended and (ii) to lack of water at the interface.[3,54] In this work, however, it was shown that LGG is able to attach on substrates regardless of their surface energy. This result is in accordance with the recent study, in which it was suggested that the surface energy alone does not allow predicting bacterial attachment, as this process is governed by multiple mechanisms including the surface interaction of extending from cell appendage molecules and gene regulation.[55] Indeed, LGG is known to possess surface appendages (pili) that play an important

role in adhesive interactions.[56] The kinetics of growth of the attached bacterial cells was also affected by the substrate properties. The slowing down of LGG growth on SAM-NH_3^+ can be attributed to transformations in polysaccharides within the biofilm, but further investigation is needed to confirm this hypothesis. Here, it is important to note that changes in LGG biofilm composition on SAM-NH_3^+ was not associated with cell death that may occur because of the ion exchange process[57] or strong electrostatic interactions with molecules essential for the survival of the bacteria.[58] The results obtained in this work indeed showed that LGG has very strong interaction forces that occur at long rupture distances on -NH_3^+ surface. However, these strong forces did not damage the LGG cell wall. It is possible that the membrane of the cell was not disrupted due to the presence of a thick peptidoglycan layer characteristic for Gram-positive bacteria, in accordance with the hypothesis of Terada *et al.*[9] and Gottenbos *et al.*[10]

A remarkable influence of the substrate functionality on the retention of attached LGG cells was observed. It was surprising to see nearly empty substrates after 2.5 hours of LGG inoculation, when these substrates were functionalized with SAM-OH and SAM-CH_3 preliminarily to LGG flow. Indeed, based on earlier findings on *P. fluorescens*[40] and on *E. coli,*[59] it was expected that high infrared integrated intensities observed for LGG during inoculation would correlate with high coverage of the surface with bacteria. It appears that LGG cells lift off from the latter substrates upon rinsing due to weak interaction with -CH_3 and -OH groups. This result is in agreement with the study reporting high forces ($\approx 10^{-7}$ N, oriented perpendicularly with respect to the substrate) induced at the interface between bacteria, liquid and air.[46] Furthermore, the influence of the substrate surfaces properties on the retention of LGG cells was also observed after 24 hours of biofilm formation. LGG cells did not succeed to develop interactions with the CH_3-terminated substrate strong enough to withstand partial rinsing even at exposure for a long time. This result

highlights how necessary it is to consider substrate properties in the experiments with biofilm formation. Indeed, as previously postulated by Frickmann *et al.*,[60] the question may arise whether the lower/higher number of recovered cells from the surface after biofilm formation is a function of lower/higher retention of the biofilm at washing before counting, or an actual decrease/increase of the number of cells in the biofilm provoked by the conditions used. From the results found in the present study, these effects seem to be of special concern when the support for biofilm formation does not provide strong adhesive interactions. For LGG, the NH_3^+-terminated substrate provided the strongest interactions while maintaining the cells intact and physiologically active. Electrostatic interactions are thus more favorable than hydrophobic and hydrophilic ones for maintaining LGG cells as sessile and active under mechanical stress conditions.

CONCLUSIONS

This paper reports the conception of alkanethiol-based functionalized ZnSe surfaces and their impact on the attachment and development of biofilms by the probiotic bacterium LGG. A combination of ATR-FTIR, EBS, and contact angle measurements put in evidence structural differences in SAMs formed onto ZnSe as a function of the terminal group ($-CH_3$, -OH, $-NH_2$) of the alkanethiol chain. These terminal groups also played role in the in the attachment of LGG cells and subsequent biofilm development. Indeed, the rate of LGG attachment was the highest on the NH_3^+-functionalized substrate. The latter substrate promoted the formation of a dense LGG biofilm after 26.5 hours. This biofilm was able to withstand the lifting force arising at rinsing, unlike the one obtained on the CH_3-functionalized substrate. The results of ATR-FTIR *in situ* measurements revealed changes in polysaccharide composition of LGG biofilm cultivated on the substrate with SAM-NH_3^+, which might have contributed in the stronger mechanical stability of the biofilm. Notably, the membrane of LGG cells stayed intact despite the strong interaction observed with the

latter substrate. In perspective, other molecules baring positive charges would be interesting to study in order to expand the application of LGG biofilms, as for example it was recently demonstrated with a cationic dextran derivative used to attach LGG cells on gold electrodes.[44]

AUTHOR INFORMATION

Corresponding Author

* E-mail: fabienne.quiles@univ-lorraine.fr

Author Contributions

The manuscript was written through contributions of all authors. All authors have given approval to the final version of the manuscript.

Funding Sources

This work was funded by Institut Carnot ICEEL.

ACKNOWLEDGMENT

The authors thank Patricia Galán (Instituto de Ciencia de Materiales de Madrid) and Jérôme Grausem (SMI Service Facility from LCPME) for technical assistance with EBS and ATR-FTIR experiments, respectively.

REFERENCES

(1) Flemming, H.-C.; Wuertz, S. Bacteria and Archaea on Earth and Their Abundance in Biofilms. *Nat. Rev. Microbiol.* **2019**, *17* (4), 247–260.
(2) Stoodley, P.; Sauer, K.; Davies, D. G.; Costerton, J. W. Biofilms as Complex Differentiated Communities. *Annu. Rev. Microbiol.* **2002**, *56* (1), 187–209.
(3) Boks, N. P.; Norde, W.; van der Mei, H. C.; Busscher, H. J. Forces Involved in Bacterial Adhesion to Hydrophilic and Hydrophobic Surfaces. *Microbiology* **2008**, *154* (10), 3122–3133.
(4) Cunliffe, D.; Smart, C. A.; Alexander, C.; Vulfson, E. N. Bacterial Adhesion at Synthetic Surfaces. *Appl. Environ. Microbiol.* **1999**, *65* (11), 4995–5002.

(5) Li, B.; Logan, B. E. Bacterial Adhesion to Glass and Metal-Oxide Surfaces. *Colloids Surf., B* **2004**, *36* (2), 81–90.
(6) Poortinga, A. T.; Bos, R.; Norde, W.; Busscher, H. J. Electric Double Layer Interactions in Bacterial Adhesion to Surfaces. *Surf. Sci. Rep.* **2002**, *47* (1), 1–32.
(7) Chen, C.; Petterson, T.; Illergård, J.; Ek, M.; Wågberg, L. Influence of Cellulose Charge on Bacteria Adhesion and Viability to PVAm/CNF/PVAm-Modified Cellulose Model Surfaces. *Biomacromolecules* **2019**, *20* (5), 2075–2083.
(8) Gottenbos, B.; van der Mei, H. C.; Busscher, H. J.; Grijpma, D. W.; Feijen, J. Initial Adhesion and Surface Growth of *Pseudomonas aeruginosa* on Negatively and Positively Charged Poly(Methacrylates). *J. Mater. Sci. Mater. Med.* **1999**, *10*, 853–855.
(9) Terada, A.; Yuasa, A.; Kushimoto, T.; Tsuneda, S.; Katakai, A.; Tamada, M. Bacterial Adhesion to and Viability on Positively Charged Polymer Surfaces. *Microbiology* **2006**, *152* (12), 3575–3583.
(10) Gottenbos, B.; Grijpma, D. W.; van der Mei, H. C.; Feijen, J.; Busscher, H. J. Antimicrobial Effects of Positively Charged Surfaces on Adhering Gram-Positive and Gram-Negative Bacteria. *J. Antimicrob. Chemother.* **2001**, *48* (1), 7–13.
(11) Hill, C.; Guarner, F.; Reid, G.; Gibson, G. R.; Merenstein, D. J.; Pot, B.; Morelli, L.; Canani, R. B.; Flint, H. J.; Salminen, S.; Calder, P. C.; Sanders, M. E. The International Scientific Association for Probiotics and Prebiotics Consensus Statement on the Scope and Appropriate Use of the Term Probiotic. *Nat. Rev. Gastroenterol. Hepatol.* **2014**, *11* (8), 506–514.
(12) Probiotics Market Size, Share & Trends Analysis Report By Application (Food & Beverages, Dietary Supplements, Animal Feed), By End-Use, By Region, And Segment Forecast, 2018 - 2024.
(13) Lebeer, S.; Verhoeven, T. L. A.; Perea Velez, M.; Vanderleyden, J.; De Keersmaecker, S. C. J. Impact of Environmental and Genetic Factors on Biofilm Formation by the Probiotic Strain *Lactobacillus rhamnosus* GG. *Appl. Environ. Microbiol.* **2007**, *73* (21), 6768–6775.
(14) Salas-Jara, M. J.; Sanhueza, E. A.; Retamal-Díaz, A.; González, C.; Urrutia, H.; García, A. Probiotic *Lactobacillus fermentum* UCO-979C Biofilm Formation on AGS and Caco-2 Cells and *Helicobacter pylori* Inhibition. *Biofouling* **2016**, *32* (10), 1245–1257.
(15) Aoudia, N.; Rieu, A.; Briandet, R.; Deschamps, J.; Chluba, J.; Jego, G.; Garrido, C.; Guzzo, J. Biofilms of *Lactobacillus plantarum* and *Lactobacillus fermentum*: Effect on Stress Responses, Antagonistic Effects on Pathogen Growth and Immunomodulatory Properties. *Food Microbiol.* **2016**, *53*, 51–59.
(16) Leccese Terraf, M. C.; Juárez Tomás, M. S.; Rault, L.; Le Loir, Y.; Even, S.; Nader-Macías, M. E. F. Biofilms of Vaginal *Lactobacillus reuteri* CRL 1324 and *Lactobacillus rhamnosus* CRL 1332: Kinetics of Formation and Matrix Characterization. *Arch. Microbiol.* **2016**, *198* (7), 689–700.
(17) Bain, C. D.; Troughton, E. B.; Tao, Y. T.; Evall, J.; Whitesides, G. M.; Nuzzo, R. G. Formation of Monolayer Films by the Spontaneous Assembly of Organic Thiols from Solution onto Gold. *J. Am. Chem. Soc.* **1989**, *111* (1), 321–335.
(18) Guo, J.-S.; Zhang, P.; Chen, Y.-P.; Shen, Y.; Hu, X.; Yan, P.; Yang, J.-X.; Fang, F.; Li, C.; Gao, X.; Wang, G.-X. Microbial Attachment and Adsorption–Desorption Kinetic of Tightly Bound Extracellular Polymeric Substances on Model Organic Surfaces. *Chem. Eng. J.* **2015**, *279*, 516–521.

(19) Pranzetti, A.; Salaün, S.; Mieszkin, S.; Callow, M. E.; Callow, J. A.; Preece, J. A.; Mendes, P. M. Model Organic Surfaces to Probe Marine Bacterial Adhesion Kinetics by Surface Plasmon Resonance. *Adv. Funct. Mater.* **2012**, *22* (17), 3672–3681.
(20) Wiencek, K. M.; Fletcher, M. Effects of Substratum Wettability and Molecular Topography on the Initial Adhesion of Bacteria to Chemically Defined Substrata. *Biofouling* **1997**, *11* (4), 293–311.
(21) Hou, J.; Veeregowda, D. H.; van de Belt-Gritter, B.; Busscher, H. J.; van der Mei, H. C. Extracellular Polymeric Matrix Production and Relaxation under Fluid Shear and Mechanical Pressure in *Staphylococcus aureus* Biofilms. *Appl. Environ. Microbiol.* **2018**, *84* (1), e01516-17.
(22) Parikh, S. J.; Mukome, F. N. D.; Zhang, X. ATR–FTIR Spectroscopic Evidence for Biomolecular Phosphorus and Carboxyl Groups Facilitating Bacterial Adhesion to Iron Oxides. *Colloids Surf., B* **2014**, *119*, 38–46.
(23) Quilès, F.; Saadi, S.; Francius, G.; Bacharouche, J.; Humbert, F. *In Situ* and Real Time Investigation of the Evolution of a *Pseudomonas fluorescens* Nascent Biofilm in the Presence of an Antimicrobial Peptide. *BBA-Biomembranes* **2016**, *1858* (1), 75–84.
(24) Noble-Luginbuhl, A. R.; Nuzzo, R. G. Assembly and Characterization of SAMs Formed by the Adsorption of Alkanethiols on Zinc Selenide Substrates. *Langmuir* **2001**, *17* (13), 3937–3944.
(25) Plyler, E. K. Infrared Spectra of Methanol, Ethanol, and n-Propanol. *J. Res. Natl. Bur. Stan.* **1952**, *48* (4), 281–286.
(26) Demissie, A. T.; Haugstad, G.; Frisbie, C. D. Quantitative Surface Coverage Measurements of Self-Assembled Monolayers by Nuclear Reaction Analysis of Carbon-12. *J. Phys. Chem. Lett.* **2016**, *7* (17), 3477–3481.
(27) Mayer, M. Improved Physics in SIMNRA 7. *Nucl. Instrum. Meth. B* **2014**, *332*, 176–180.
(28) Fowkes, F. M. Additivity of Intermolecular Forces at Interfaces. I. Determination of the Contribution to Surface and Interfacial Tensions of Dispersion Forces in Various Liquids. *J. Phys. Chem.* **1963**, *67* (12), 2538–2541.
(29) Yunda, E.; Quilès, F. *In Situ* Spectroscopic Analysis of *Lactobacillus rhamnosus* GG Flow on an Abiotic Surface Reveals a Role for Nutrients in Biofilm Development. *Biofouling* **2019**, *35* (5), 494–507.
(30) Delille, A.; Quilès, F.; Humbert, F. *In Situ* Monitoring of the Nascent *Pseudomonas Fluorescens* Biofilm Response to Variations in the Dissolved Organic Carbon Level in Low-Nutrient Water by Attenuated Total Reflectance-Fourier Transform Infrared Spectroscopy. *Appl. Environ. Microbiol.* **2007**, *73* (18), 5782–5788.
(31) Burgain, J.; Scher, J.; Lebeer, S.; Vanderleyden, J.; Corgneau, M.; Guerin, J.; Caillet, C.; Duval, J. F. L.; Francius, G.; Gaiani, C. Impacts of PH-Mediated EPS Structure on Probiotic Bacterial Pili–Whey Proteins Interactions. *Colloids Surf., B* **2015**, *134*, 332–338.
(32) Porter, M. D.; Bright, T. B.; Allara, D. L.; Chidsey, C. E. D. Spontaneously Organized Molecular Assemblies. 4. Structural Characterization of n-Alkyl Thiol Monolayers on Gold by Optical Ellipsometry, Infrared Spectroscopy, and Electrochemistry. *J. Am. Chem. Soc.* **1987**, *109* (12), 3559–3568.
(33) te Riet, J.; Smit, T.; Coenen, M. J. J.; Gerritsen, J. W.; Cambi, A.; Elemans, J. A. A. W.; Speller, S.; Figdor, C. G. AFM Topography and Friction Studies of Hydrogen-Bonded Bilayers of Functionalized Alkanethiols. *Soft Matter* **2010**, *6* (15), 3450–3454.

(34) Wang, H.; Chen, S.; Li, L.; Jiang, S. Improved Method for the Preparation of Carboxylic Acid and Amine Terminated Self-Assembled Monolayers of Alkanethiolates. *Langmuir* **2005**, *21* (7), 2633–2636.
(35) Fears, K. P.; Creager, S. E.; Latour, R. A. Determination of the Surface p*K* of Carboxylic- and Amine-Terminated Alkanethiols Using Surface Plasmon Resonance Spectroscopy. *Langmuir* **2008**, *24* (3), 837–843.
(36) Khan, M. Md. T.; Ista, L. K.; Lopez, G. P.; Schuler, A. J. Experimental and Theoretical Examination of Surface Energy and Adhesion of Nitrifying and Heterotrophic Bacteria Using Self-Assembled Monolayers. *Environ. Sci. Technol.* **2011**, *45* (3), 1055–1060.
(37) Arima, Y.; Iwata, H. Effects of Surface Functional Groups on Protein Adsorption and Subsequent Cell Adhesion Using Self-Assembled Monolayers. *J. Mater. Chem.* **2007**, *17* (38), 4079–4087.
(38) Berron, B.; Jennings, G. K. Loosely Packed Hydroxyl-Terminated SAMs on Gold. *Langmuir* **2006**, *22* (17), 7235–7240.
(39) Suci, P. A.; Vrany, J. D.; Mittelman, M. W. Investigation of Interactions between Antimicrobial Agents and Bacterial Biofilms Using Attenuated Total Reflection Fourier Transform Infrared Spectroscopy. *Biomaterials* **1998**, *19* (4–5), 327–339.
(40) Quilès, F.; Humbert, F.; Delille, A. Analysis of Changes in Attenuated Total Reflection FTIR Fingerprints of *Pseudomonas fluorescens* from Planktonic State to Nascent Biofilm State. *Spectrochim. Acta A* **2010**, *75* (2), 610–616.
(41) Kang, S.-Y.; Bremer, P. J.; Kim, K.-W.; McQuillan, A. J. Monitoring Metal Ion Binding in Single-Layer *Pseudomonas* a*eruginosa* Biofilms Using ATR−IR Spectroscopy. *Langmuir* **2006**, *22* (1), 286–291.
(42) Stuart, B. H. *Infrared Spectroscopy: Fundamentals and Applications*; John Wiley & Sons: Chichester, West Susex, England, 2004.
(43) Tripathi, P.; Beaussart, A.; Alsteens, D.; Dupres, V.; Claes, I.; von Ossowski, I.; de Vos, W. M.; Palva, A.; Lebeer, S.; Vanderleyden, J.; Dufrêne, Y. F. Adhesion and Nanomechanics of Pili from the Probiotic *Lactobacillus rhamnosus* GG. *ACS Nano* **2013**, *7* (4), 3685–3697.
(44) Jarosz, M.; Grudzień, J.; Kamiński, K.; Gawlak, K.; Wolski, K.; Nowakowska, M.; Sulka, G. D. Novel Bioelectrodes Based on Polysaccharide Modified Gold Surfaces and Electrochemically Active *Lactobacillus rhamnosus* GG Biofilms. *Electrochim. Acta* **2019**, *296*, 999–1008.
(45) Busscher, H. J.; van der Mei, H. C. Microbial Adhesion in Flow Displacement Systems. *Clin. Microbiol. Rev.* **2006**, *19* (1), 127–141.
(46) Gómez-Suárez, C.; Busscher, H. J.; van der Mei, H. C. Analysis of Bacterial Detachment from Substratum Surfaces by the Passage of Air-Liquid Interfaces. *Appl. Environ. Microbiol.* **2001**, *67* (6), 2531–2537.
(47) Beaussart, A.; El-Kirat-Chatel, S.; Herman, P.; Alsteens, D.; Mahillon, J.; Hols, P.; Dufrêne, Y. F. Single-Cell Force Spectroscopy of Probiotic Bacteria. *Biophys. J.* **2013**, *104* (9), 1886–1892.
(48) Zhang, X.; Wang, L.; Levänen, E. Superhydrophobic Surfaces for the Reduction of Bacterial Adhesion. *RSC Adv.* **2013**, *3* (30), 12003–12020.
(49) Love, J. C.; Estroff, L. A.; Kriebel, J. K.; Nuzzo, R. G.; Whitesides, G. M. Self-Assembled Monolayers of Thiolates on Metals as a Form of Nanotechnology. *Chem. Rev.* **2005**, *105* (4), 1103–1170.

(50) te Riet, J.; Smit, T.; Gerritsen, J. W.; Cambi, A.; Elemans, J. A. A. W.; Figdor, C. G.; Speller, S. Molecular Friction as a Tool to Identify Functionalized Alkanethiols. *Langmuir* **2010**, *26* (9), 6357–6366.
(51) Lacour, V.; Moumanis, K.; Hassen, W. M.; Elie-Caille, C.; Leblois, T.; Dubowski, J. J. Formation Kinetics of Mixed Self-Assembled Monolayers of Alkanethiols on GaAs(100). *Langmuir* **2019**, *35* (13), 4415–4427.
(52) KRÜSS GmbH Technical Note. So You Want to Measure Surface Energy? Models for Surface Free Energy Calculation, https://Www.Kruss-Scientific.Com/Services/Education-Theory/Literature/Application-Reports/.
(53) Oh, J. K.; Yegin, Y.; Yang, F.; Zhang, M.; Li, J.; Huang, S.; Verkhoturov, S. V.; Schweikert, E. A.; Perez-Lewis, K.; Scholar, E. A.; Taylor, T. M.; Castillo, A.; Cisneros-Zavallos, L.; Min, Y.; Akbulut, M. The Influence of Surface Chemistry on the Kinetics and Thermodynamics of Bacterial Adhesion. *Sci. Rep.* **2018**, *8* (1), 17247.
(54) Tuson, H. H.; Weibel, D. B. Bacteria–Surface Interactions. *Soft Matter* **2013**, *9* (17), 4368–4380.
(55) Alexander, M. R.; Williams, P. Water Contact Angle Is Not a Good Predictor of Biological Responses to Materials. *Biointerphases* **2017**, *12* (2), 02C201.
(56) Segers, M. E.; Lebeer, S. Towards a Better Understanding of *Lactobacillus rhamnosus* GG - Host Interactions. *Microb. Cell. Fact.* **2014**, *13* (Suppl 1), S7.
(57) Kügler, R.; Bouloussa, O.; Rondelez, F. Evidence of a Charge-Density Threshold for Optimum Efficiency of Biocidal Cationic Surfaces. *Microbiology* **2005**, *151* (5), 1341–1348.
(58) Bieser, A. M.; Tiller, J. C. Mechanistic Considerations on Contact-Active Antimicrobial Surfaces with Controlled Functional Group Densities. *Macromol. Biosci.* **2011**, *11* (4), 526–534.
(59) Freudenthal, O.; Quilès, F.; Francius, G. Discrepancies between Cyclic and Linear Antimicrobial Peptide Actions on the Spectrochemical and Nanomechanical Fingerprints of a Young Biofilm. *ACS Omega* **2017**, *2* (9), 5861–5872.
(60) Frickmann, H.; Klenk, C.; Warnke, P.; Redanz, S.; Podbielski, A. Influence of Probiotic Culture Supernatants on in Vitro Biofilm Formation of Staphylococci. *Eur. J. Microbiol. Immunol.* **2018**, *8* (4), 119–127.